

Wolfgang Schattke, Michel A. Van Hove (Eds.)

Solid-State Photoemission and Related Methods

Theory and Experiment



WILEY-
VCH

WILEY-VCH GmbH & Co. KGaA

This Page Intentionally Left Blank

Wolfgang Schattke, Michel A. Van Hove (Eds.)

Solid-State Photoemission and Related Methods

Theory and Experiment

Wolfgang Schattke, Michel A. Van Hove (Eds.)

Solid-State Photoemission and Related Methods

Theory and Experiment



WILEY-
VCH

WILEY-VCH GmbH & Co. KGaA

Editors

Prof. Wolfgang Schattke
Universität Kiel, Germany
schattke@tp.cau.de

Prof. Michel A. Van Hove
Lawrence Berkeley National Laboratory, USA
VanHove@lbl.gov

This book was carefully produced. Nevertheless, authors, editors and publisher do not warrant the information contained therein to be free of errors. Readers are advised to keep in mind that statements, data, illustrations, procedural details or other items may inadvertently be inaccurate.

**Library of Congress Card No.: applied for
British Library Cataloging-in-Publication Data:**

A catalogue record for this book is available from the British Library

**Bibliographic information published by
Die Deutsche Bibliothek**

Die Deutsche Bibliothek lists this publication in the Deutsche Nationalbibliografie; detailed bibliographic data is available in the Internet at <<http://dnb.ddb.de>>.

Cover Picture

Photoelectron angular distributions of 1T-TiTe₂ taken at 100 eV photon energy (showing the momentum resolved electronic structure over several Brillouin zones). Top sheet: Fermi level. Sheets to higher binding energies separated by 100 meV.

© 2003 WILEY-VCH GmbH & Co. KGaA,
Weinheim

All rights reserved (including those of translation into other languages). No part of this book may be reproduced in any form – nor transmitted or translated into machine language without written permission from the publishers. Registered names, trademarks, etc. used in this book, even when not specifically marked as such, are not to be considered unprotected by law.

Printed in the Federal Republic of Germany
Printed on acid-free paper

Composition Uwe Krieg, Berlin
Printing Strauss Offsetdruck GmbH, Mörlenbach
Bookbinding Litges & Dopf Buchbinderei
GmbH, Heppenheim

ISBN 3-527-40334-5

Preface

The objective of this volume is to provide a comprehensive review of the state and progress of solid-state photoemission, including closely-related methods, both from a theoretical and from an experimental point of view. This material should be of particular interest to a wide range of theoretical and experimental physicists, materials scientists, and chemists, from graduate students to experts, dealing especially with surfaces and other nanostructures.

Many excellent treatments of major aspects of this field have appeared in the last decade: we mention in particular Inglesfield and Plummer's 1992 review article¹, which focused on the fundamental principles of valence-level angle-resolved photoemission, and the 1995 book by Hüfner², which adopted a more experimental perspective.

This field has continued to grow at a fast pace on many fronts, greatly expanding its capabilities and achievements. We thus felt that it was necessary and timely to bring together diverse developments in a single monograph, in an attempt to provide a degree of up-to-date completeness of the current state of the art.

Given that photoemission is intimately tied to ground and excited electronic states, this book starts with an exposition of contemporary theory of such states. It then provides a unified overview of the theoretical principles of core and valence photoemission. This is then followed by a much more thorough treatment of the theory of core level photoemission.

Turning to valence photoemission, a chapter is devoted to valence bands and VUV spectra, while another addresses actual development of spatial imaging of valence levels besides the traditional spectroscopic analysis. The very important application to the study of magnetic materials is covered in the following chapter. In the subsequent chapter, recent progress towards a compact photoemission program based on an all-electron ab-initio representation is described in the context of band structure theory.

Several very exciting novel developments with two-particle spectroscopies and their inherent access to many-particle properties such as lifetime and correlation are introduced in three separate chapters dealing with: time-resolved two-photon photoemission; low-energy (e,2e) spectroscopy; and one-photon two-electron transitions at surfaces.

The book next shifts the attention toward the use of core levels, in particular for surface structure determination. For that purpose, an overview of the known structures of surfaces is offered, being fundamental to many surface processes, including photoemission itself.

¹ J. E. Inglesfield and E. W. Plummer, *The physics of photoemission* in S. D. Kevan (ed.) *Angle-resolved photoemission*, (Elsevier 1992)

² S. Hüfner, *Photoelectron spectroscopy* in Springer Series in Solid State Sciences, Vol. 82 (Springer, Berlin 1995)

This is followed by a very recent application of core-level angle resolved photoelectron spectroscopy to surface structural analysis; its implications for the valence band structure are also discussed. Then, new holographic approaches to obtaining surface structure are addressed.

Several related methods of surface analysis are covered next. One is X-ray absorption fine structure and its derivative techniques. Another is the use of X-rays and their properties in photoemission and X-ray emission. Finally, developments in low-energy electron diffraction are addressed in the last chapter, covering the important issue of surface vibrations.

Wolfgang Schattke and Michel A. Van Hove, Editors

August 2003

In memoriam Lars Hedin (1930–2002)

Tragically, soon after completing his chapter for this Handbook, Professor Lars Hedin passed away.

Lars was born in 1930 and raised in Örebro, Sweden. He met and within one year married his lifetime companion Hillevi in 1953. They now have three daughters and six grandchildren. His higher education was at the Royal Institute of Technology in Stockholm, Uppsala University, and finally Chalmers University of Technology in Gothenburg, from which he obtained his Ph.D. in 1965. He then became Professor of Physics at Linköping University (1970–71), and subsequently at Lund University (1971–95), where he spent most of his career. During his years in Lund, he made extended visits to Stanford, Nijmegen, and Yokohama. He was head of a theory group at the Max Planck Institute in Stuttgart from 1994–98, at which time he returned to Lund as Professor Emeritus, and continued to maintain an active research program until his death. Beyond this, Lars was an editor of *Solid State Communications* (1971–90), played a leading role in the organization of the International Conferences on Vacuum Ultraviolet Radiation Physics (1977–92), and was a member of many other committees and editorial boards in Sweden and abroad.

The field of condensed matter theory has been enriched by Lars' many outstanding and fundamental contributions over the last half century. He is responsible for various important advances, particularly in the theory of interacting electron systems. These began in the 1960s, the fascinating period during which many of the analytical tools of many body theory were being developed. His contributions took place in parallel with the development of various powerful spectroscopic tools for studying complex electronic systems, and Lars provided crucial insights for linking theory with experiment, as illustrated in his chapter for this Handbook. His theoretical developments demonstrate his unique ability to combine mathematical rigor and physical intuition within formal analytical frameworks which he designed. A multitude of scientific milestones testify to his profound impact. In particular, Lars' theories paved the way for a quantitative understanding of electronic excitations, in particular in photoemission and X-ray absorption spectra. These theories provide the basis for many calculations of electronic structure and for a quantitative understanding of experimental investigations that now dominate the science of the microscopic world.

Those who personally know him will agree that Lars combined a most friendly and engaging personality with an exacting scientific attitude that made him a great researcher, teacher, and friend. We are most grateful for having received Lars' manuscript in time for inclusion in this Handbook. It reflects most of the topics he was devoted to, especially in the last few years of his very productive life. As such it represents one of his last scientific achievements, and it also provides a solid foundation for many of the topics covered in the Handbook. By dedicating this Handbook to Lars Hedin, we hope to show how very much alive his influence will remain within the scientific community.

Wolfgang Schattke and Michel A. Van Hove

Contents

Preface	V
In Memoriam Lars Hedin (1930–2002)	VII
List of contributors	XVII
1 Electronic structure theory for ground and excited state properties of materials	
(<i>A.J. Freeman, R. Asahi, A. Continenza, and R. Wu</i>)	1
1.1 Introduction	1
1.2 Density functional theory and the FLAPW method	3
1.2.1 Introduction	3
1.2.2 Density-functional theory	3
1.2.3 The FLAPW basis-set	5
1.3 Electronic structure theory for excited states	6
1.3.1 Band gaps and derivative discontinuities	6
1.3.2 Band gaps and nonlocal potentials	9
1.3.3 Quasiparticle calculations	10
1.3.4 Density functional theory using non-local functionals	14
1.4 Application to semiconductor materials	22
1.4.1 Bulk semiconductor materials	22
1.4.2 Semiconductor/semiconductor interfaces	25
1.4.3 Semiconductor/metal interfaces	28
1.5 Applications of the first-principles FLAPW approach to studies of magnetism	31
1.5.1 Magnetism	31
1.5.2 Magneto-crystalline anisotropy in thin films.	32
1.5.3 Higher-order magneto-crystalline anisotropy	34
1.5.4 Magnetostriction	36
1.5.5 Magneto-optical effects	40
1.5.6 Magnetic circular dichroism	40
References	42

2 Overview of core and valence photoemission	
(<i>W. Schattke, M.A. Van Hove, F.J. García de Abajo, R. Díez Muiño, and N. Mannella</i>)	50
2.1 Introduction	50
2.2 Green function methods	52
2.2.1 Photoemission and the many-body problem	52
2.2.2 Green functions and one-particle Schrödinger equation	54
2.2.3 Elementary excitations in systems of interacting particles	58
2.2.4 The self-energy	60
2.2.5 Independent particle states and related methods	61
2.2.6 Perturbation expansion	65
2.2.7 Diagrams in many-body systems	68
2.2.8 Spectral representation	72
2.2.9 Photocurrent	77
2.3 Three-step model versus one-step model	83
2.4 Golden Rule	85
2.4.1 Linear response in the external field	85
2.4.2 Dipole approximation	86
2.5 Initial state	88
2.5.1 Core levels	88
2.5.2 Valence bands	89
2.6 Final state	93
2.6.1 Direct solution of Schrödinger equation	94
2.6.2 Multiple scattering method	99
2.7 Matrix elements: core versus valence levels	102
2.8 Optical effects	104
2.8.1 Resonant photoemission	104
2.8.2 Photoemission by surface optical response fields	105
2.9 Spin effects	107
2.10 Computer codes for photoelectron diffraction and spectroscopy	109
References	112
3 General theory of core electron photoemission	
(<i>L. Hedin</i>)	116
3.1 Introduction	116
3.2 Theory	121
3.2.1 General considerations	121
3.2.2 A model Hamiltonian with a priori determined parameters	123
3.2.3 Extrinsic and intrinsic losses in core electron photoemission	126
3.2.4 Charge transfer and shake-down satellites	134
3.2.5 Resonant photoemission	136
3.2.6 Phonons and temperature effects	138
3.3 Concluding remarks	138
References	139

4	Valence band VUV spectra	141
	<i>(I. Bartoš and W. Schattke)</i>	
4.1	Introduction	141
4.2	Electrons at crystal surfaces	141
4.2.1	One-electron approach	142
4.2.2	Many-electron approach	143
4.3	Photoelectron spectroscopy	144
4.3.1	Band mapping (peak positions)	145
4.3.2	Electron and hole lifetimes (peak widths)	148
4.3.3	Orbital orientation (peak intensities)	150
4.3.4	EDC spectra (profiles)	151
4.4	Summary	156
	References	156
5	Angle-resolved photoelectron spectroscopy: From photoemission imaging to spatial resolution	159
	<i>(K. Roßnagel, L. Kipp, and M. Skibowski)</i>	
5.1	Introduction	159
5.2	Angle-resolved photoemission	160
5.3	Experimental considerations	161
5.4	Photoemission imaging: TiTe_2 as a test case	162
5.5	Three-dimensional Fermi surface mapping: NbSe_2	170
5.6	Spatial origin of photoelectrons: $\text{GaAs}(110)$ surface states	170
5.7	Angle-resolved photoelectron nanospectroscopy	172
5.8	Conclusions	174
	References	175
6	Electronic states of magnetic materials	177
	<i>(F.J. Himpsel and K.N. Altmann)</i>	
6.1	Introduction	177
6.2	Band structure of magnetic materials	178
6.2.1	Mapping of energy bands	178
6.2.2	Ferromagnetic metals	183
6.2.3	Antiferromagnetic metals	190
6.2.4	Magnetic alloys	190
6.3	Magnetic insulators	193
6.3.1	Magnetic superconductors	198
6.3.2	Half-metals	200
6.3.3	Magnetic semiconductors	202
6.4	Phase transitions	204
6.4.1	Ferromagnets	204
6.4.2	Antiferromagnets	206
6.5	Magnetic multilayers	206
6.5.1	Quantum well states	206
6.5.2	Oscillatory coupling	209

6.6	Magnetoelectronics	210
6.6.1	Giant magnetoresistance (GMR) and spin-polarized tunneling	211
6.6.2	Spin scattering and magnetic doping	212
	References	214
7	The band structure theory of LEED and photoemission	220
	(<i>E.E. Krasovskii</i>)	
7.1	Introduction	220
7.2	Ultima ratio regnum: the APW method	221
7.2.1	The augmented plane waves formalism	222
7.2.2	Andersen's LAPW	223
7.2.3	The extended LAPW - $\mathbf{k}\cdot\mathbf{p}$ method	226
7.2.4	Back to plane waves	227
7.3	Electron diffraction in semi-infinite crystals	229
7.3.1	Inverse band structure problem	229
7.3.2	Matching the solutions at the crystal surface	230
7.3.3	Embedding	233
7.3.4	Current attenuation and current conservation	235
7.4	Is band structure a legitimate concept at high energies?	237
7.4.1	Target current spectroscopy of NbSe ₂	238
7.4.2	Photoemission from the surface state on the Al (100) surface	242
	References	244
8	Time-resolved two-photon photoemission	247
	(<i>Th. Fauster</i>)	
8.1	Basics of two-photon photoemission	247
8.1.1	Energy diagram	247
8.1.2	Energy-resolved spectroscopy	247
8.1.3	Time-resolved measurements	248
8.1.4	Variation of photon energy	250
8.1.5	Experimental setup	251
8.2	Theoretical description of two-photon photoemission	253
8.2.1	Coupling between electron and hole	253
8.2.2	Phase coherence	253
8.3	Bulk properties	257
8.3.1	Direct bulk transitions	257
8.3.2	Lifetimes of hot electrons	258
8.4	Surface properties	260
8.4.1	Surface states	260
8.4.2	Image-potential states	262
8.4.3	Adsorbate states	264
8.5	Outlook	265
	References	265

9 Low-energy (e,2e) spectroscopy	269
(<i>R. Feder and H. Gollisch</i>)	
9.1 Introduction	269
9.2 Setup and basic concepts	270
9.3 Theory	272
9.3.1 Framework	272
9.3.2 Approximations and computational aspects	273
9.3.3 Selection rules	275
9.4 Prototypical spectra	276
9.5 Electron scattering dynamics	278
9.5.1 Elastic one-electron reflection	278
9.5.2 Pair diffraction and coulomb correlation	280
9.6 Valence electronic structure	282
9.6.1 Surface sensitivity and surface states	282
9.6.2 Symmetry resolution by selection rules	285
9.7 Spin-polarized (e,2e) spectroscopy	287
9.7.1 Non-magnetic surfaces	287
9.7.2 Ferromagnetic surfaces	289
References	291
10 One-photon two-electron transitions at surfaces	295
(<i>N. Fominykh, J. Berakdar, J. Henk, S. Samarin, A. Morozov, F. U. Hillebrecht, J. Kirschner, and P. Bruno</i>)	
10.1 Introduction	295
10.2 General considerations	296
10.2.1 The single-particle Green's function	296
10.2.2 The two-particle Green's function	298
10.3 Photo-induced double-electron emission	300
10.3.1 Experimental details	301
10.3.2 Pathways for the electron-pair emission	302
10.4 Numerical realization and experimental results	304
10.4.1 Simple model calculations	304
10.4.2 Numerical scheme with a realistic single-particle band structure	306
10.4.3 Numerical results for the angular pair correlation in Cu(001)	307
10.4.4 Energy-correlation functions	308
10.5 Conclusions	310
References	310
11 Overview of surface structures	313
(<i>M.A. Van Hove</i>)	
11.1 Introduction	313
11.2 Techniques of surface structure determination	314
11.2.1 Diffraction techniques	315
11.2.2 Scattering techniques	318
11.2.3 Microscopic and topographic techniques	318

11.3	Two-dimensional ordering	318
11.3.1	Ordering principles at surfaces	319
11.3.2	Nomenclature	319
11.4	Clean surfaces	321
11.4.1	Bulk-like lattice termination	322
11.4.2	Stepped surfaces	323
11.4.3	Relaxations	323
11.4.4	Reconstruction	324
11.4.5	Surface segregation	325
11.4.6	Quasicrystals	325
11.5	Adsorbate-covered surfaces	325
11.5.1	Physisorption	326
11.5.2	Atomic chemisorption sites and bond lengths	326
11.5.3	Atomic multilayers	328
11.5.4	Molecular adsorption	329
11.5.5	Adsorbate-induced relaxations	331
11.5.6	Adsorbate-induced reconstructions	331
11.5.7	Compound formation and surface segregation	333
	References	334

12 Angle resolved photoelectron spectroscopy:

From traditional to two-dimensional photoelectron spectroscopy

(*H. Daimon, F. Matsui, and K. Sakamoto*) **338**

12.1	Experiment – semiconductors	338
12.1.1	Photoemission from semiconductor surfaces	338
12.1.1.1	Introduction	338
12.1.1.2	Ordered overlayers on semiconductor surfaces	339
12.1.1.3	Initial stage of oxidation of the Si(111)-(7×7) surface	345
12.2	Two-dimensional photoelectron spectroscopy	347
12.2.1	Two-dimensional photoelectron diffraction stereograph	347
12.2.1.1	Display-type spherical mirror analyzer	348
12.2.1.2	Structure analysis by two-dimensional photoelectron diffraction, holography	349
12.2.1.3	Surface photoelectron diffraction	350
12.2.1.4	Bulk photoelectron diffraction	352
12.2.1.5	Photoelectron holography	352
12.2.1.6	Circularly polarized-light photoelectron diffraction	353
12.2.1.7	Peak rotation and the orbital angular momentum	354
12.2.1.8	Stereograph by circular dichroism in photoelectron angular distribution	357
12.2.1.9	Stereoscopic photographs	357
12.2.1.10	Stereo photograph of atomic arrangement	358
12.2.1.11	Stereo microscope	360
12.2.2	Two-dimensional photoelectron spectroscopy of valence band	361
12.2.2.1	Photoelectron angular distribution from valence band	361

12.2.2.2	Determination of atomic orbitals composing Fermi surface	361
12.2.2.3	Three dimensional band dispersion of graphite	362
	References	366
13	Holographic surface crystallography: Substrate as reference	
	<i>(R.J. Harder and D.K. Saldin)</i>	370
13.1	Introduction	370
13.2	Surface crystallography as a structure completion problem	371
13.3	Maximum entropy algorithm for surface crystallography	372
13.3.1	Surface X-ray diffraction	372
13.3.2	Low energy electron diffraction	375
13.4	Discussion and conclusions	382
	References	384
14	XAFS and related methods: Theoretical techniques	
	<i>(J.J. Rehr, R.C. Albers, and A.L. Ankudinov)</i>	387
14.1	Introduction	387
14.2	Standard one-electron theory of X-ray spectra	388
14.2.1	Theoretical considerations	388
14.2.2	Golden rule	389
14.2.3	Green's Function formalism	390
14.2.4	Multiple-scattering theory	391
14.2.5	Scattering potentials	391
14.2.6	Self energy and mean free path	392
14.3	Applications to X-ray spectroscopies	392
14.3.1	EXAFS	392
14.3.2	XANES	395
14.3.3	Atomic-XAFS	396
14.3.4	Photoelectron diffraction	396
14.3.5	Other spectroscopies	397
14.4	Many-body effects	397
14.4.1	Inelastic losses	397
14.4.2	Extrinsic losses	397
14.4.3	Intrinsic losses	397
14.4.4	Interference between extrinsic and intrinsic losses	399
14.4.5	EXAFS amplitude reduction factor S_0^2	400
14.4.6	Local field effects	400
14.5	Conclusions	401
	References	401
15	X-ray optics, standing waves, and interatomic effects in photoemission and X-ray emission	
	<i>(Ch.S. Fadley, S.-H. Yang, B.S. Mun, and F.J. García de Abajo)</i>	404
15.1	Introduction	404
15.2	Non-resonant X-ray optical effects in photoemission	404

15.2.1	Background and first applications in the total reflection geometry . . .	404
15.2.2	Standing wave effects for probing buried interface and nanostructures	406
15.3	Resonant X-ray optical effects and multi-atom resonant photoemission	417
15.3.1	General considerations	417
15.3.2	Resonant X-ray optical theory	417
15.3.3	An alternative viewpoint: multiatom resonant photoemission (MARPE)	420
15.4	X-ray optical effects in X-ray emission and resonant inelastic scattering . . .	427
15.5	Concluding remarks and future directions	428
	References	430
16	Thermal vibrations at surfaces analyzed with LEED	
	<i>(W. Moritz and J. Landskron)</i>	433
16.1	Introduction	433
16.2	Thermal vibration in the kinematic theory of diffraction	434
16.2.1	Harmonic vibrations	436
16.2.2	Anharmonic vibrations	438
16.3	Multiple scattering theory	439
16.3.1	Calculation of the multipole expansion coefficients	443
16.4	Discussion	449
16.5	Applications	450
16.5.1	Cu(110)	450
16.5.2	CO/Ru(001)	453
16.6	Summary	455
	References	457
	Appendix	
	Color figures	461
	Index	473

List of contributors

- *R.C. Albers*
Theoretical Division
Los Alamos National Laboratory
Los Alamos
NM 87545
USA
- *K.N. Altmann*
Department of Physics and SRC
University of Wisconsin Madison
1150 University Ave.
Madison, WI 53706-1390
USA
- *A.L. Ankudinov*
Department of Physics
University of Washington
Seattle
WA 98195-1560
USA
- *Ryoji Asahi*
Toyota Central R&D Labs., Inc.
Nagakute
Aichi 480-1192
Japan
- *I. Bartoš*
Institute of Physics
Academy of Sciences of the Czech Republic
Cukrovarnická 10
162 53 Prague 6
Czech Republic
e-mail: bartos@fzu.cz
- *J. Berakdar*
Max-Planck-Institut für Mikrostrukturphysik
Weinberg 2
D-06120 Halle (Saale)
Germany
e-mail: jber@mpi-halle.mpg.de
- *P. Bruno*
Max-Planck-Institut für Mikrostrukturphysik
Weinberg 2
D-06120 Halle (Saale)
Germany
- *Alessandra Continenza*
Istituto Nazionale di Fisica della Materia and
Università dell'Aquila
L'Aquila
Italy
- *Hiroshi Daimon*
Graduate School of Materials Science
Nara Institute of Science and Technology
8916-5 Takayama, Ikoma, Nara
630-0192 Japan
e-mail: daimon@ms.aist-nara.ac.jp
- *R. Díez Muiño*
Donostia International Physics Center
(DIPC)
Paseo Manuel de Lardizabal 4,
20018 San Sebastián, Spain
e-mail: wabdimur@sq.ehu.es

- *Charles S. Fadley*
 Department of Physics
 University of California Davis
 Davis, CA 95616 USA
 and
 Materials Sciences Division
 Lawrence Berkeley National Laboratory
 Berkeley CA 94720 USA
 e-mail: fadley@lbl.gov
- *Thomas Fauster*
 Lehrstuhl für Festkörperphysik
 Universität Erlangen-Nürnberg
 Staudtstr. 7
 D-91058 Erlangen
 Germany
 e-mail: fauster@fkp.physik.uni-erlangen.de
- *R. Feder*
 Theoretische Festkörperphysik
 Universität Duisburg
 D-47048 Duisburg
 Germany
 e-mail: feder@dagobert.uni-duisburg.de
- *N. Fominykh*
 Max-Planck-Institut für Mikrostrukturphysik
 Weinberg 2
 D-06120 Halle (Saale)
 Germany
- *A.J. Freeman*
 Department of Physics and Astronomy
 Northwestern University
 Evanston, IL
 e-mail: art@pluto.phys.nwu.edu
- *F.J. García de Abajo*
 Centro Mixto CSIC-UPV/EHU,
 Apartado 1072,
 20080 San Sebastián, Spain
- and
 Donostia International Physics Center
 (DIPC)
 Paseo Manuel de Lardizabal 4,
 20018 San Sebastián, Spain
 e-mail: jga@sc.ehu.es
- *H. Gollisch*
 Theoretische Festkörperphysik
 Universität Duisburg
 D-47048 Duisburg
 Germany
- *R.J. Harder*
 Department of Physics and Laboratory for
 Surface Studies
 University of Wisconsin-Milwaukee
 P. O. Box 413
 Milwaukee, WI 53201
 USA
- *Lars Hedin*
 Dept. of Physics
 University of Lund
 Sölvegatan 14A, 22362 Lund,
 Sweden
 and
 MPI-FKF
 Heisenbergstrasse 1
 D-70569 Stuttgart
 Germany
- *J. Henk*
 Max-Planck-Institut für Mikrostrukturphysik
 Weinberg 2
 D-06120 Halle (Saale)
 Germany
- *F.U. Hillebrecht*
 Max-Planck-Institut für Mikrostrukturphysik
 Weinberg 2
 D-06120 Halle (Saale)
 Germany

- *Franz J. Himpsel*
Department of Physics
University of Wisconsin Madison
1150 University Ave.
Madison, WI 53706-1390
USA
e-mail: fhimpse1@facstaff.wisc.edu
- *Lutz Kipp*
Institut für Experimentelle und Angewandte
Physik
Christian-Albrechts-Universität
Leibnizstraße 19
D-24098 Kiel
Germany
e-mail: kipp@physik.uni-kiel.de
- *J. Kirschner*
Max-Planck-Institut für Mikrostrukturphysik
Weinberg 2
D-06120 Halle (Saale)
Germany
- *E.E. Krasovskii*
Institut für Theoretische Physik und
Astrophysik
Christian-Albrechts-Universität
Leibnizstr.15
D-24098 Kiel
Germany
e-mail: krasovsk@tp.cau.de
- *J. Landskron*
Department of Earth and Environmental
Sciences
Section Crystallography
University of Munich
Theresienstr. 41
80333 Munich
Germany
- *N. Mannella*
Materials Sciences Division and Advanced
Light Source
Lawrence Berkeley National Laboratory
Berkeley, CA 94720
USA
e-mail: norman@electron.lbl.gov
- and
Department of Physics
University of California
Davis, CA 95616, USA
- *Fumihiko Matsui*
Graduate School of Materials Science
Nara Institute of Science and Technology
8916-5 Takayama, Ikoma, Nara
630-0192 Japan
- *Wolfgang Moritz*
Department of Earth and Environmental
Sciences
Section Crystallography
University of Munich
Theresienstr. 41
80333 Munich
Germany
e-mail:
Wolfgang.Moritz@lrz.uni-muenchen.de
- *A. Morozov*
Max-Planck-Institut für Mikrostrukturphysik
Weinberg 2
D-06120 Halle (Saale)
Germany
- *Bongjin Simon Mun*
Materials Sciences Division and Advanced
Light Source
Lawrence Berkeley National Laboratory
Berkeley CA 94720
USA

- *J.J. Rehr*
Department of Physics
University of Washington
Seattle
WA 98195-1560
USA
e-mail: jjr@leonardo.phys.washington.edu
- *Kai Roßnagel*
Institut für Experimentelle und Angewandte
Physik
Christian-Albrechts-Universität
Leibnizstraße 19
D-24098 Kiel
Germany
e-mail: rossnagel@physik.uni-kiel.de
- *Kazuyuki Sakamoto*
Department of Physic
Graduate School of Science
Tohoku University
Sendai, 980-8578, Japan
e-mail: sakamoto@surface.phys.tohoku.ac.jp
- *D.K. Saldin*
Department of Physics and Laboratory for
Surface Studies
University of Wisconsin-Milwaukee
P. O. Box 413
Milwaukee, WI 53201
USA
e-mail: dksaldin@uwm.edu
- *S. Samarin*
Max-Planck-Institut für Mikrostrukturphysik
Weinberg 2
D-06120 Halle (Saale)
Germany
- *Wolfgang Schattke*
Institut für Theoretische Physik und
Astrophysik
Christian-Albrechts-Universität
Leibnizstr. 15
D-24098 Kiel
Germany
e-mail: schattke@tp.cau.de
- *Michael Skibowski*
Institut für Experimentelle und Angewandte
Physik
Christian-Albrechts-Universität
Leibnizstraße 19
D-24098 Kiel
Germany
- *Michel A. Van Hove*
Materials Sciences Division and Advanced
Light Source
Lawrence Berkeley National Laboratory
Berkeley, CA 94720
USA
e-mail: vanhove@lbl.gov
and
Department of Physics
University of California at Davis
Davis, CA 95616
USA
- *Ruqian Wu*
Department of Physics and Astronomy
University of California
Irvine
CA 92697-4575
- *See-Hun Yang*
IBM Almaden Research Center
San Jose, CA 95120 USA
e-mail: shyang@electron.lbl.gov

1 Electronic structure theory for ground and excited state properties of materials

Arthur J. Freeman, Ryoji Asahi, Alessandra Continenza, and Ruqian Wu

1.1 Introduction

It is now well recognized that recent major advances in the quantitative computation of ground-state properties in solids are essentially related to the development of density-functional theory (DFT) in the local density approximation (LDA) and the local spin density approximation (LSDA). [1, 2] These efficient approximation schemes give the electronic ground-state energy and density distribution as a function of the position of the atomic nuclei, which in turn determine the molecular and crystal structure and give the forces acting on the atomic nuclei when they are not at their equilibrium positions. The LDA (or LSDA) has been widely used to solve problems in atomic, molecular, and condensed matter physics, such as phase transitions, vibration spectra, chemical reactions, and magnetic properties.

Recent advances in experimental techniques such as X-ray absorption and inverse photoemission strongly require understanding of unoccupied states by first-principles calculations in addition to the occupied states. Although excitation properties are outside the domain of DFT, LDA eigenvalues have been frequently interpreted as quasiparticle states. This is because LDA is so widely used and much easier to perform than full many-body theories. In practice, LDA band structures successfully give an account of experiment including some excitation properties, *e.g.*, photoemission spectra of metals. This procedure, however, is certainly not valid for all the eigenvalues and excitation properties.

One of the major problems in describing excitation properties is that the LDA gives a substantial underestimate of the band gap in semiconductors and insulators, typically by 40–50% in comparison with experiment. This problem, the so-called band gap problem, is so serious when considering fundamental properties in semiconductors for instance, that it has been intensively discussed over 20 years. A complication of the problem comes from the difficulty to access an exact form of the exchange-correlation functional or the corresponding exchange-correlation potential in the Kohn Sham (KS) scheme.

Several attempts have been undertaken to set up alternatives to LDA in order to improve LDA and to extend its applicability to excitation properties. These can be divided into mainly two groups. One is to obtain the quasiparticle energies, which directly correspond to the excitation energies of a many-body Dyson equation, by the perturbation expansion of the self-energy. A comprehensive discussion including a more realistic approximation, known as the *GW* approximation, to the self-energy was given by Hedin [3]. Another theoretical approach in going beyond LDA is to attempt to find better energy functionals by modeling the exchange-correlation hole but still within DFT framework; this includes the self-interaction correction

(SIC), [4] the LDA+U, [5] and the optimized effective potential (OEP) method, [6–8] the generalized density functional theory, [9–11] and the generalized Kohn-Sham (GKS) scheme with the screened-exchange LDA method [12, 13] (sX-LDA).

The simplification of the GW calculation, called the model GW method, [14, 15] is one way to reduce the numerical effort of the GW calculations. Although the accuracy should be limited by the neglect of local-field effects and dynamic screening, the results for various nonmagnetic semiconductors [14] and for transition metal oxides [15–18], give mostly good agreement with experiment and the results of full GW calculations. While the method gives self-consistent eigenvalues and wavefunctions with respect to the perturbed self-energy corrections, the reliability of the total energy, and therefore of the ground states obtained, has not been established.

The applicability of the SIC and the LDA+U approaches is relatively limited to the particular systems where localized states are involved. The LDA+U works reasonably well for the Mott-Hubbard insulators or rare-earth metal compounds, where the partially filled $3d$ or $4f$ bands are split by the Coulomb interaction, forming the upper and lower Hubbard bands. The SIC also describes the Mott-Hubbard insulators and the $3d$ monoxides. However, these methods fail to give satisfactory results for more itinerant systems; in particular, the SIC does not yield good band gaps of sp semiconductors, *e.g.*, Si and Ge. [19]

The basic idea of the OEP method was proposed [6] by Sharp and Horton in 1953, showing the way to obtain a local exchange potential exactly from the Hartree-Fock potential. The method was revised to improve the LDA description. Kotani [7] used the OEP with the correlation energy in the random-phase approximation (RPA) and presented results for Cu, Fe, Co, Ni, Si, and MnO. The results for metals are very close to those of LDA, and a good agreement with experiment is obtained for MnO. However, the band gap of Si is improved by only 0.2 eV. Städele *et al.* suggested [8] that a main effect for improvement of the band gap by the OEP method is a self-interaction reduction, not including the discontinuity of the exchange-correlation potential which is supposed to be dominant for Si. [20]

The screened-exchange LDA method (sX-LDA) was first proposed [12] by Bylander and Kleinman in order to obtain a better band gap. Seidl *et al.* showed [13] that the method is actually described in the framework of the generalized Kohn-Sham scheme (GKS), and that the discontinuity of the exchange-correlation potential is introduced through the nonlocal screened potential. Encouraging results for the band gaps, structural properties, and optical properties were demonstrated for several bulk semiconductor materials. [12, 13, 21–23] The method was also applied to surface and superlattice. [24] The advantages of the sX-LDA over the GW calculations are that it is much less computationally demanding, and that it permits the self-consistent determination of ground-state properties.

In this chapter, after a short introduction to density functional theory and its most precise implementation via the full-potential linearized augmented plane wave (FLAPW) method, we present a brief discussion on the general aspects of the band gap problem and its prescriptions, theoretical frameworks of the model GW and the sX-LDA are presented. The former is derived from the quasiparticle picture through the GW approximation, and the latter is introduced as a particular case of the generalized KS scheme. These two methods have a capability to obtain self-consistent properties including band gaps in a wide range of semiconductors. Moreover, rather light computational demands allows us to implement them into an all-electron methods, the FLAPW method. The applications of these method are also demonstrated in the case of semiconductor and magnetic properties.

1.2 Density functional theory and the FLAPW method

1.2.1 Introduction

The full-potential spin-polarized linear augmented plane wave (FLAPW) method is considered to be the most accurate electronic structure calculation scheme. It has its origin in the augmented plane wave (APW) method introduced by Slater [25] (details about this method can also be found in Ref. [26]). In this approach, real space is partitioned into spherical regions around atoms (“muffin-tins” or “atomic spheres”) and interstitial regions between the spheres. Computationally, the APW method is demanding since the basis functions are energy dependent and the eigenvalue problem non-linear. The subsequent linearization of the APW method (LAPW) [27, 28], where the energy dependence is removed by selecting a fixed set of suitable muffin-tin radial functions and their energy derivatives, represented an important development. In the full-potential (F)LAPW method there is no shape approximation for either the charge density or the potential, and all electrons are treated in the self-consistent process; the core electrons are treated fully relativistically and the valence electrons are treated semi-relativistically. Further details can be found in original papers [29, 30] and in recent reviews [31, 32].

Aside from the early important introduction of a total energy capability [33], recent improvements and extensions to the present FLAPW calculation scheme include: (i) evaluation of forces on the atoms, which affords automatic optimization of the atomic geometry [34–36], (ii) methodological developments resulting in significant speed-ups [37], (iii) spin-orbit coupling affording calculation of magnetic properties, namely, magnetocrystalline anisotropy (MCA), surface magneto-optic Kerr effect (SMOKE), and magnetic circular X-ray dichroism (MCD), (iv) optical properties, (v) the option of several different exchange-correlation functionals, i.e., the local density approximation (LDA) and the generalized gradient approximation (GGA) and (vi) the treatment of excited states via screened exchange (sX), as well as model *GW* treatments, and (vii) the calculation of vibrational frequencies. A very recent and important break-through is the successful implementation of a parallelized version of the code.

1.2.2 Density-functional theory

The FLAPW method employs density-functional theory (DFT), introduced by Hohenberg and Kohn [38] and Kohn and Sham [39]. The underlying theorem (Hohenberg-Kohn-Sham theorem) on which this theory rests is that the total energy, E , of an atomistic system can be expressed as a functional of its electron density, ρ , namely, $E = E[\rho]$, that E is at its minimum for the ground-state density, and is stationary with respect to first-order variations in the density.

Typically, the Born-Oppenheimer approximation [40] is employed which assumes that the motion of the nuclei are negligible with respect to that of electrons. This implies that the electronic structure is calculated for a given atomic geometry; the nuclei are then moved according to classical mechanics.

The Kohn-Sham equations

To obtain the ground-state density, the variational principle is applied with respect to the one-particle wave functions:

$$\left[(-\hbar^2/2m)\nabla^2 + V_{eff}(\mathbf{r})\right]\psi_i(\mathbf{r}) = \varepsilon_i\psi_i(\mathbf{r}), \quad (1.1)$$

where

$$V_{eff}(\mathbf{r}) = V_C(\mathbf{r}) + \mu_{xc}[\rho(\mathbf{r})] \quad (1.2)$$

is the effective potential and ε_i the effective one-electron eigenvalues. Equations (1.1) are the ‘‘Kohn-Sham equations’’ and the solutions, $\psi_i(\mathbf{r})$, form an orthonormal set, i.e., $\int \psi_i^*(\mathbf{r})\psi_j(\mathbf{r}) d\mathbf{r} = \delta_{ij}$. The Coulomb or electrostatic potential is given as:

$$V_C(\mathbf{r}) = -e^2 \sum_{\alpha} \frac{Z_{\alpha}}{|\mathbf{r} - \mathbf{R}_{\alpha}|} + e^2 \int \frac{\rho(\mathbf{r}')}{|\mathbf{r} - \mathbf{r}'|} d\mathbf{r}' \quad (1.3)$$

which can also be calculated using Poisson’s equation, i.e.,

$$\nabla^2 V_C(\mathbf{r}) = -4\pi e^2 q(\mathbf{r}) \quad , \quad (1.4)$$

where $q(\mathbf{r})$ represents the electronic charge distribution *and* the positive point charges at position \mathbf{R}_{α} . The exchange-correlation potential is given by

$$\mu_{xc} = \partial E_{xc}[\rho]/\partial \rho \quad . \quad (1.5)$$

Because the exchange-correlation potential (and energy) are not known, approximations have to be made.

Spin-polarized density functional theory

The generalization of density-functional theory to spin-polarized systems has been made within the local spin density approximation (LSD) [41, 42]. The important quantity, in addition to the electron density $\rho(\mathbf{r})$, is the spin density $\sigma(\mathbf{r})$ which is the density difference between the spin-up and spin-down configurations, i.e., $\sigma(\mathbf{r}) = \rho_{\uparrow}(\mathbf{r}) - \rho_{\downarrow}(\mathbf{r})$; the total density being given by $\rho(\mathbf{r}) = \rho_{\uparrow}(\mathbf{r}) + \rho_{\downarrow}(\mathbf{r})$. Because the exchange-correlation potential for spin-up and spin-down electrons is in general different, the spin-polarized form of the Kohn-Sham equations are:

$$\left[(-\hbar^2/2m)\nabla^2 + V_{eff}^{\sigma}(\mathbf{r})\right]\psi_i^{\sigma}(\mathbf{r}) = \varepsilon_i^{\sigma}\psi_i^{\sigma}(\mathbf{r}), \quad \text{where } \sigma = \uparrow \text{ or } \downarrow \quad , \quad (1.6)$$

and

$$V_{eff}^{\sigma}(\mathbf{r}) = V_C(\mathbf{r}) + \mu_{xc}^{\sigma}[\rho(\mathbf{r}), \sigma(\mathbf{r})] \quad . \quad (1.7)$$

Thus there are two sets of single-particle wave functions, one for spin-up (or ‘‘majority’’) electrons and one for spin-down (‘‘minority’’) electrons, each with corresponding one-electron eigenvalues.

Exchange-correlation functions

Local-density approximation (LDA) A very successful and widely used approximation for the exchange-correlation energy is the local-density approximation (LDA). Here the exchange-correlation energy is assumed to depend only on the local electron density of each volume element $d\mathbf{r}$:

$$E_{xc}[\rho] \approx \int \rho(\mathbf{r})\varepsilon_{xc}[\rho(\mathbf{r})]d\mathbf{r} \quad (1.8)$$

$\varepsilon_{xc}[\rho]$ is the exchange-correlation energy per electron of a *homogeneous* electron gas and is expressed as an analytic function of the electron density, as is the exchange-correlation potential, μ_{xc} . There are various forms of the LDA in the literature; we refer to those of Hedin-Lunqvist [43] and Wigner (non-spin-polarized forms), and Barth-Hedin [41] (spin-polarized form) since they are the ones implemented in the present FLAPW program version.

Generalized gradient approximation (GGA) In recent years, the generalized gradient approximation (GGA) is being considered as a possible improvement over the LDA. The GGA has been found to generally improve the description of total energies, ionization energies, and electron affinities of atoms, atomization energies of molecules [44–46] and some solid state properties [47–50]. Adsorption energies of adparticles on surfaces are also reported to be improved [51, 52] as are reaction energies [53, 54]. Furthermore, the GGA leads to significantly better activation energy barriers for H_2 dissociation [55, 56] and also the relative stability of structural phases appears to be better described for magnetic [57] and non-magnetic systems [58, 59].

There are a number of GGA approaches in the literature. The generic form of the GGA exchange-correlation energy may be written as:

$$E_{xc}^{\text{GGA}}[\rho] = \int \rho(\mathbf{r})\varepsilon_{xc}^{\text{GGA}}(\rho(\mathbf{r}), \nabla\rho(\mathbf{r}))d\mathbf{r} \quad (1.9)$$

so that it depends locally on the electronic density $\rho(\mathbf{r})$ and its gradient.

The GGA developed by Perdew and Wang (PW) [44] is derived essentially from first principles, combining the gradient expansions of the exchange and correlation holes of a non-uniform electron gas with real-space truncations to enforce constraints imposed by properties of the physical exchange-correlation hole. The GGA developed by Becke and Perdew [60] on the other hand relies on fitted parameters. In the present program version of the FLAPW program the GGA implemented is that proposed by Perdew, Burke and Ernzerhof (PBE) [61]. This functional is regarded to be conceptually more concise than the PW GGA but appears to yield very similar results [62].

1.2.3 The FLAPW basis-set

In the FLAPW method, in bulk material, real space is partitioned into spherical regions around atoms (“muffin-tins” or “atomic spheres”) and interstitial regions between the spheres. In the spherical region, the basis functions are products of radial functions and spherical harmonics, and in the interstitial region plane waves are used. For the film geometry, there is a number

of atomic layers surrounded by vacuum, thus in addition to spherical and interstitial regions, one defines a vacuum region, which starts at $\pm D/2$ and ends at $\pm \tilde{D}/2$ (see Fig. 1.1), where the wave functions are products of two-dimensional (2D) plane waves and z -dependent functions which are solutions of the one-dimensional Schrödinger equation of the (x, y) -averaged potential in the vacuum region.

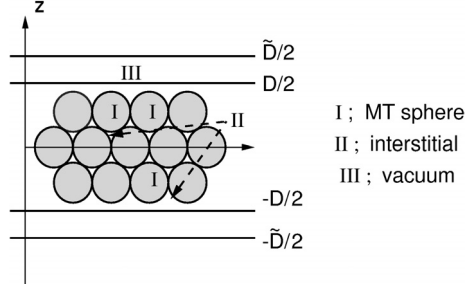


Figure 1.1: Geometry for a film calculation showing division of space in a film geometry.

Specifically, the FLAPW one-particle wave functions in the film geometry are:

$$\psi_i(\mathbf{r}, \mathbf{k}_{\parallel}) = \sum_j c_{ij} \phi(\mathbf{r}, \mathbf{K}_j); \quad \mathbf{K}_j = \mathbf{k}_{\parallel} + \mathbf{G}_j, \quad (1.10)$$

where \mathbf{k}_{\parallel} is an arbitrary vector of the 2D BZ and \mathbf{G}_j is a three-dimensional (3D) reciprocal lattice vector (in the z -direction an artificial periodicity between the boundaries at $\pm \tilde{D}/2$ is imposed). The basis functions are:

$$\phi(\mathbf{r}, \mathbf{K}_j) = \begin{cases} \Omega^{-1/2} e^{i\mathbf{K}_j \cdot \mathbf{r}} & \text{interstitial} \\ \sum_{lm} [A_{lm}^{\alpha}(\mathbf{K}_j) u_l(E_l^{\alpha}, r_{\alpha}) + B_{lm}^{\alpha}(\mathbf{K}_j) \dot{u}_l(E_l^{\alpha}, r_{\alpha})] Y_{lm}(\hat{r}_{\alpha}) & \text{sphere} \\ \sum_q [A_q(\mathbf{K}_j) u_{\mathbf{k}q}(E_{\nu}, z) + B_q(\mathbf{K}_j) \dot{u}_{\mathbf{k}q}(E_{\nu}, z)] e^{i(\mathbf{k}_{\parallel} + \mathbf{K}_q^{\parallel}) \cdot \mathbf{r}} & \text{vacuum} \end{cases} \quad (1.11)$$

The Coulomb potential $V(\mathbf{r})$ is obtained by solving Poisson's equation in each of the three regions. At infinity the potential is gauged equal to zero in the case of the film geometry. The effective single-particle potential is constructed by adding the exchange-correlation potential, which is determined by the charge density in real space and transformation of it into each representation. The core electrons are treated fully relativistically and are updated at each iteration using a scheme for *free* atoms (only the spherical part of the potential is used). The valence electrons are expanded in a variational basis set and are treated scalar-relativistically.

1.3 Electronic structure theory for excited states

1.3.1 Band gaps and derivative discontinuities

The band gap is rigorously defined as the difference between the lowest conduction-band energy and the highest valence-band energy: the latter is the energy required to remove an electron from the insulating N -particle ground state to infinity, *i.e.*, the ionization potential, I ;

- spectral density matrix 82
- spectral function 75, 76, 83, 148, 166, 184, 269, 273, 275, 283, 296, 298, 400
- spectral representation 54, 72, 153, 297, 300
- spectral weight 75
- spectromicroscopy 417
- spectroscopic factor 297, 300
- spin analysis 270
- spin current 190, 210
- spin density matrix 92
- spin density wave 210
- spin detection 177
- spin distribution 189
- spin effects 107
- spin excitation 178
- spin filter 192, 210, 211
- spin fluctuation 124
- spin magnetic dipole operator 41
- spin polarization 51, 92, 107, 110, 212, 270, 272, 273, 287, 289, 290
- spin polarized photoemission 182
- spin reflector 210
- spin scattering 212
- spin selectivity 213
- spin tunneling current 202
- spin wave 182, 183
- spin-dependent mean free path 212
- spin-dependent phase shift 110
- spin-dependent potential barrier 208
- spin-dependent reflectivity 208
- spin-dependent reflectivity of interfaces 210
- spin-dependent scattering 211
- spin-dependent scattering dynamics 270
- spin-dependent step 209
- spin-flip transition 182
- spin-orbit 107, 108, 390, 397
- spin-orbit coupling 272, 275, 276, 288, 291
- spin-orbit coupling effect 270
- spin-orbit interaction 182, 287, 356
- spin-polarization 180, 189, 198, 200, 202, 208
- spin-polarized (e,2e) spectroscopy 287
- spin-polarized current 202
- spin-polarized impurity 190
- spin-polarized inverse photoemission 182
- spin-polarized LEED 288
- spin-polarized photoemission 189, 201, 208
- spin-polarized quantum well state 212
- spin-polarized scanning tunneling microscopy 189
- spin-polarized state 201
- spin-polarized tunneling 178, 211
- spin-polarized tunneling device 212
- spin-resolved layer density of states 273
- spin-resolved photocurrent 92
- spin-resolved photoemission 188
- spin-scattering at the surface 200
- spin-selective elastic scattering 193
- spin-selective scattering 190, 213
- spintronic 177
- SPLEED *see* spin-polarized LEED
- split position 449
- Sr₂RuO₄ 362
- standing wave 404, 406, 411, 412, 416, 419, 427–429
- standing wave excitation 417
- standing wave formation 409
- standing wave generator 412, 469
- standing-wave excited photoemission 415
- step barrier 143
- stepped surface 323
- stereo microscope 360, 361, 467
- stereo microscopy of atomic arrangement 347
- stereo photograph 358
- stereo photograph of atomic arrangement 358
- stereograph by circular dichroism 357
- stereographic image 308, 309
- stereographic projection 350
- stereoscopic photograph 357
- stereoscopic recognition 348
- STM *see* scanning tunneling microscopy
- Stoner criterion 204
- Stoner excitation 183
- Stoner gap 182, 183, 185
- strain-induced uniaxial 37
- strong correlations 124
- strongly correlated system 136, 139
- structural complexity of the unit cell 384
- structural parameter 453, 454
- structure analysis 349
- structure completion problem 371, 373
- structure factor 371, 372, 381, 426
- structure factor amplitude 374, 377
- structure factor of a unit cell 376
- structure factor of the bulk 376
- structure parameter 434
- substitutional atom 327
- substitutional compound 333
- substitutional defect 345

- substrate 313, 378, 384, 408
- substrate as reference 370
- substrate lattice 321
- substrate-adsorbate bond 313
- successive approximation 54, 66
- successive iteration 55
- sudden 116
- sudden approximation 82, 83, 122, 398, 399
- sudden removal of the core electron 121
- sum rule 41, 74
- summation over most divergent terms 129
- superconducting hole 200
- superconducting rare earth compound 198
- superconductivity 204, 206
- superlattice 190, 313, 320, 328, 378
- superstructure 343, 345
- superstructure rods 372
- superstructures of surface layers 384
- surface 404
- surface band structure 93, 340
- surface barrier 142, 143
- surface composition 318
- surface core shift 118
- surface core-level shift 341
- surface crystal structure 382
- surface crystallography 150, 316, 383
- surface electron structure 142
- surface ferromagnetism 205
- surface Green function 142
- surface magneto-optic Kerr effect 3
- surface melting 450
- surface optical response 105
- surface ordering 319
- surface phase transition 433
- surface photoelectron diffraction 350
- surface plasmon satellite 131
- surface plasmons 129
- surface potential 93
- surface properties 260
- surface reciprocal-lattice vector 375
- surface reconstruction 153, 433
- surface relaxation 321
- surface resonance 142
- surface response 106
- surface scattering of the electromagnetic wave 106
- surface segregation 325, 331, 333
- surface sensitivity 141, 144, 282, 316, 370, 419, 427, 433
- surface state 142–145, 148, 150, 159, 179, 180, 189, 235, 242, 243, 251, 260, 261, 269, 270, 274, 275, 282, 339, 340
- surface state dispersion 344
- surface structure 313, 319, 321, 382
- surface structure determination 109
- surface topography 318
- surface unit cell 372
- surface X-ray crystallography 371
- surface X-ray diffraction 371, 372, 433
- surface-parallel wave vector 160
- surface-perpendicular component of the wave vector 168
- surface-perpendicular wave vector 160
- SWG *see* standing wave generator
- sX-LDA method 14
 - applications 18
- symmetry 87, 178, 180, 181, 185, 188, 200, 201, 307, 361, 363, 447, 450
- symmetry of the atomic orbital 362
- symmetry resolution 270, 285
- synchrotron 107
- synchrotron light source 182, 252
- synchrotron radiation 118, 138, 141, 144, 163, 180, 301, 316, 317, 349, 361
- synchrotron radiation X-ray sources 388
- T-matrix 439, 440
- target current spectroscopy 153, 238
- target structure factor 373
- TCS *see* target current spectroscopy
- TDLDA *see* time-dependent local density approximation
- TDS *see* thermal diffuse scattering
- temperature 342
- temperature dependence of the vibration amplitude 454
- temperature dependent atomic scattering matrix 443
- temperature dependent I/V curves 450
- temperature dependent LEED 453
- temperature effects 138, 451
- temperature factor 433, 434, 436, 446, 455
- ternary III-V semiconductor alloys 22
- thermal diffuse scattering 434–436
- thermal disorder 395
- thermal ellipsoid 438, 443, 446, 449
- thermal expansion 438

- thermal vibration 388, 389, 433
- thermal vibration at surfaces 433
- thin film 185, 189, 205
- thin magnetic film 206
- Thomas-Fermi limit 305
- Thomas-Fermi screening length 274
- three step model 117
- three-current correlation function 116, 126
- three-step 116
- three-step formulation 51
- three-step model 83, 141, 145
- threshold 132
- time delay 247
- time evolution 56, 67, 68
- time ordering operator 297
- time resolution 301
- time window 301
- time-dependent local density approximation (TDLDA) 400
- time-dependent population 254
- time-inversed scattering state 126
- time-of-flight 301
- time-of-flight detection 252
- time-of-flight distribution 277
- time-of-flight technique 270, 271
- time-ordered Green function 65
- time-resolved measurements 248
- time-resolved technique 149
- time-resolved two-photon photoemission 247
- time-resolved two-photon spectroscopy 149
- time-reversed LEED state 80, 82, 84, 118, 121, 123, 128
- time-reversed relativistic LEED state 273
- time-scale 116
- Ti:sapphire laser 251
- TiSe₂ 106
- TiSe₂(0001) 108
- TiTe₂ 93, 96, 99, 159, 162–165, 167, 168
- TiTe₂(0001) 94, 98, 462, 463
- torque method 34
- total current spectroscopy 97
- total energy band 277, 278
- total energy diagram 195
- total energy distribution 278
- total reflection 104, 404, 406, 419, 428
- transition 345
- transition amplitude 125, 128, 137
- transition metal 188, 189, 194
- transition metal alloy 190
- transition metal compounds 135, 195
- transition metal oxide 177, 195, 200
- transition operator 51, 354
- transition-metal oxides 295
- translation formula of spherical harmonics 100
- translational period 154
- translational periodicity 151
- translational symmetry 142, 153
- transmission 84
- transport 180, 182
- transport measurement 201
- triangulation 145
- trilayer 209, 211
- truncation of the series expansion 375
- tuneable synchrotron radiation 168
- tunneling magnetoresistance 212
- two independent photoelectron current 306
- two-body operator 63
- two-body potential 63
- two-dimensional display-type spherical mirror analyzer 361
- two-dimensional energy distribution 277
- two-dimensional free electron gas 282
- two-dimensional ordering 318
- two-dimensional periodicity 319
- two-dimensional photoelectron diffraction 348, 349
- two-dimensional photoelectron spectroscopy 338, 347
 - of valence band 361
- two-dimensional time-of-flight distribution 276, 277
- two-dimensional valence band analysis 348
- two-electron Dirac equation 272, 273
- two-electron energy correlation function 305
- two-electron photoemission 52
- two-electron photoemission spectroscopy 271
- two-hole excitation 184
- two-particle Green's function 298, 307
- two-particle propagator 300
- two-particle spectral function 300
- two-photoelectron current 302, 304–306, 309
- two-photon photoemission 148, 247
- two-photon photoemission involving bulk states 257
- two-step process 139
- ultraviolet photoelectron spectroscopy 145

- uncertainty 374, 377
- unoccupied band structure 242
- unoccupied state 141
- UPS *see* ultraviolet photoelectron spectroscopy
- vacuum ultraviolet regime 107
- vacuum-solid interface 417
- valence band 89, 144, 347, 362
- valence band electronic structure 345
- valence band offset 25
- valence band photoelectron spectroscopy 338
- valence band photoemission 345
- valence band spectra 89, 345
- valence band structure 361
- valence band VUV spectra 141
- valence band width 13, 19
- valence bandstructure 90
- valence electronic structure 270
- valence level 102
- valence level spectroscopy 84
- valence photoemission 50, 100
- valence state 51
- valence-level emission 110
- valence-to-continuum photoemission 187
- VBO *see* valence band offset
- VBW *see* valence band width
- vector potential 77, 78, 85, 106
- velocity 144, 192, 202, 210, 362, 365
- vertex 69, 72
- vertex function 299
- vertex part 72
- vertex renormalization 79
- very low energy electron diffraction 97
- very low energy electron spectroscopy 153
- vibration amplitude 452, 453, 457
- vibration frequency 330
- vibrations 111, 342
- vicinal surface 323
- VLEED *see* very low energy electron diffraction
- VUV 107, 144
- VUV excitation 151
- VUV range 98
- VUV region 109
- W(001) 276–282, 288, 289
- W(001) energy sharing curve 280
- W(001) work function 278
- W(001)-O p(2x1) 282
- W(110) 358
- W(110)1 × 12-O 350, 351, 353
- wave function 146, 207, 209, 213, 227
- wave function based method 389
- wavefunction 94, 97, 462
- wavelength 207
- wavevector 365
- wedge technique 210
- white lines 394
- Wick's theorem 67, 78
- width 141
- Wood notation 320
- work function 73, 77, 143, 181, 248, 260, 261
- X-ray absorption 387
- X-ray absorption fine structure 317, 387, 392, 399
- X-ray absorption near edge spectroscopy 391, 392, 395, 396
- X-ray absorption spectroscopy 407
- X-ray crystallography 372
- X-ray diffraction 316, 384
- X-ray emission 404, 427, 428
- X-ray excitation 150, 151
- X-ray fluorescence 428
- X-ray inelastic scattering 404
- X-ray interaction 427
- X-ray magnetic linear dichroism 209
- X-ray natural circular dichroism 397
- X-ray optical analysis 417
- X-ray optical approach 427
- X-ray optical calculation 409–411, 414, 415, 420, 423, 429
- X-ray optics 404, 409, 427
- X-ray penetration depth 407
- X-ray photoelectron diffraction 172, 387, 388, 396, 406
- X-ray spectra 388
- X-ray standing waves 317
- X-ray structure analysis 434
- X-ray transition 428
- XAFS *see* X-ray absorption fine structure
- XANES *see* X-ray absorption near edge spectroscopy
- XAS *see* X-ray absorption
- XMLD *see* X-ray magnetic linear dichroism
- XNCD *see* X-ray natural circular dichroism
- XPD *see* X-ray photoelectron diffraction